The effective conductivity of random checkerboards

Helsing, Johan

Published in:
Journal of Computational Physics

DOI:
10.1016/j.jcp.2010.10.033

2011

The effective conductivity of random checkerboards[☆]

Johan Helsing[1]

Numerical Analysis, Centre for Mathematical Sciences,
Lund University, Box 118, SE-221 00 LUND, Sweden

Abstract

An algorithm is presented for the fast and accurate solution of the electrostatic equation on multi-component random checkerboards. It relies on a particular choice of integral equation, extended as to separate ill-conditioning due to singular fields in corners from ill-conditioning due to interaction of clusters of well-conducting squares at large distances. Two separate preconditioners take care of the two separate phenomena. In a series of numerical examples, effective conductivities are computed for random checkerboards containing up to 10^4 squares with conductivity ratios of up to 10^6. The achievable relative precision in these examples is on the order of 10^{-11}.

Keywords: Integral equation, Corner singularity, Fast solver, Effective conductivity, Checkerboard

1. Introduction

A composite material of great interest in theoretical materials science is the conducting checkerboard – a material constructed from a single unit cell tiled with squares of different conductivities and repeated as to cover the entire plane. Determining the effective conductivity of such a checkerboard is a classic problem.

Checkerboard problems are, in general, very challenging. Especially so when there is a large number of squares in the unit cell and when their con-

[☆]This work was supported by the Swedish Research Council under contract 621-2007-6234.

Email address: helsing@maths.lth.se (Johan Helsing)
URL: http://www.maths.lth.se/na/staff/helsing/ (Johan Helsing)
[1]Tel.:+46 46 2223372

ductivities are randomly chosen from a wide distribution, see Section 1 of [9] and Section 5 of [24]. From a PDE point of view one first has to solve an elliptic boundary value problem in the unit cell with doubly periodic boundary conditions on the outer boundaries and continuity conditions on the internal boundaries. Then one has to evaluate a functional on the solution. The internal boundaries meet at quadruple-junctions (four-wedge corners), where strongly singular fields may arise. See Theorem 3.1 and Section 6 of [1] for the difficulties encountered within the framework of the finite element method. Nevertheless, remarkably simple closed-form expressions for the effective conductivity of two-component ordered checkerboards were found a long time ago [7, 18, 20]. This has inspired a search for closed-form solutions also for more complex arrangements. See [3, 5, 6, 21, 22] for examples where ordered checkerboards with up to four different components have been treated.

Random checkerboards are of interest in percolation theory. It is important to know how effective transport properties evolve as well-conducting squares are about to form a connected path through the unit cell. Traditionally, such investigations have been undertaken via crude mappings of continuum composites into resistor networks. Recently, qualitative studies performed with the finite element method on large two-component random checkerboards suggest that such mappings lead to a spurious secondary percolation threshold and shifts in scaling exponents and effective properties [4].

Difficulties with large random checkerboards at high contrast ratios do not just include the resolution of local fields close to quadruple-junctions, but also ill-conditioning caused by long-range interaction between clusters of well conducting components. This ill-conditioning further limits the achievable accuracy and tends to slow down the convergence of iterative solvers. It is known as *critical slowing down* in the physics community but can, for network models, be counterbalanced using multigrid methods [8].

This paper presents an integral equation based algorithm which offers high accuracy solutions to general checkerboard problems. The algorithm has three main features

- a particular choice of integral equation
- the use of recursive compressed inverse preconditioning [15, 16] to resolve layer densities in the vicinity of quadruple-junctions
- a Schur complement style preconditioner to deal with long-range interaction

Combined, these features offer tremendous increase in achievable precision and tractable system size, compared to competing methods. The algorithm can be seen as an extension of a previous algorithm [15] for elliptic problems on domains with corners and triple-junctions (three-wedge corners). In [15] we solved electrostatic problems in high-contrast granular materials with up to 900 grains. As we shall see in the present paper, the comparative advantages with recursive compressed inverse preconditioning are even more pronounced in the presence of quadruple-junctions. Furthermore, the long-range preconditioner will completely curb the critical slowing down and we can accurately solve the electrostatic equation on checkerboards with 10^4 squares of wildly varying conductivities in the unit cell using an ordinary workstation.

The paper is organized in three main sections, each treating one of the features listed above. The algorithmic presentation is mixed with numerical examples, performed in the MATLAB environment (version 7.6) and executed on an ordinary workstation equipped with an IntelCore2 Duo E8400 CPU at 3.00 GHz and 4GB of memory. The integral equations are discretized with a Nyström scheme based on composite 16-point Gauss–Legendre quadrature. The GMRES iterative solver [23] with a low-threshold stagnation avoiding technique [14] is used for the main linear systems and the stopping criterion threshold is set to machine epsilon (ϵ_{mach}). The system matrices and their action on vectors are computed explicitly in the smaller examples. The fast multipole method [13], coded in C, is used in the larger examples. See Section 4.1 of [13] and Section 3 of [11] for how to impose periodic boundary conditions on potential fields due to charges in a unit cell.

2. Integral equations for the checkerboard problem

Let the unit cell $D_0 = [-1/2, 1/2)\times[-1/2, 1/2)$ be tiled with N_{sq} equisized squares with conductivities σ_k, $k = 1, \ldots, N_{\text{sq}}$, so that the local conductivity $\sigma(r)$ at position $r = (r_x, r_y)$ is a piecewise constant function. Let the unit cell be periodically repeated as to cover the entire plane D. We need to refer to different subsets of the interfaces between the squares. The interfaces that belong to the unit cell are denoted Γ_0 and given orientation, see Fig. 1 where Γ_0 is indicated by solid lines. The interfaces Γ_0 and their periodic images are denoted Γ. The boundary of D_0 is denoted L_0. Let $\Gamma_1 = \Gamma_0 \cap L_0$, let Γ_2 be $L_0 \setminus \Gamma_1$, and let $n_r = n(r)$ be the outward unit normal of Γ at r.

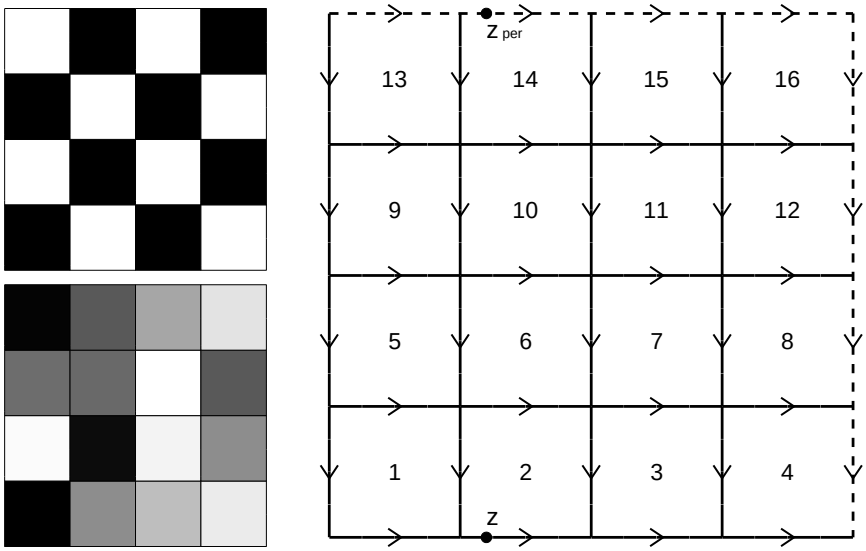

Figure 1: Top left: A part of a two-component ordered checkerboard. Bottom left and right: A unit cell D_0 of a multi-component random checkerboard with $N_{\rm sq} = 16$ numbered squares. Orientation of the interfaces Γ_0 (solid lines) and Γ_2 (dashed lines) along with a point $z \in \Gamma_1$ and its corresponding periodic image $z_{\rm per} \in \Gamma_2$.

An average electric field $e = (e_x, e_y)$ of unit strength is applied to the checkerboard and we seek the potential $U(r)$ for the ultimate computation of the effective conductivity in direction e of the checkerboard

$$\sigma_{\rm eff} = \int_{D_0} (\sigma(r) \nabla U(r) \cdot e) \, {\rm d}V_r \,, \tag{1}$$

where ${\rm d}V_r$ is an infinitesimal element of area. The average electric field e will be applied in the y-direction in all our numerical examples. To keep the notation short we make no distinction between points or vectors in a real plane $\mathbb{R}^2$ and points in a complex plane $\mathbb{C}$. All points, from now on, will be denoted z or τ.

Clearly, the local conductivity $\sigma(z)$ jumps as Γ is crossed. Let $\sigma_+(z)$ denote the conductivity on the positive side of Γ at z, let $\sigma_-(z)$ denote the

conductivity on the negative side of Γ at z, and introduce

$$a(z) = \sigma_+(z) - \sigma_-(z)\,, \quad z \in \Gamma\,, \tag{2}$$
$$b(z) = \sigma_+(z) + \sigma_-(z)\,, \quad z \in \Gamma\,, \tag{3}$$
$$c(z) = \sigma_+(z)\sigma_-(z)\,, \quad z \in \Gamma\,, \tag{4}$$
$$\lambda(z) = a(z)/b(z)\,, \quad z \in \Gamma\,. \tag{5}$$

We also need a function $l_0(z)$ on Γ_0

$$l_0(z) = \begin{cases} z - z_{\rm per}\,, & z \in \Gamma_1\,, \\ 0\,, & z \in \Gamma_0 \setminus \Gamma_1\,. \end{cases} \tag{6}$$

Here $z_{\rm per}$ is the position of the periodic image of $z \in \Gamma_1$ on Γ_2, that is, $l_0(z)$ on Γ_1 is either minus one or minus the imaginary unit, see Fig. 1. The periodic extension of $l_0(z)$ to Γ is denoted $l(z)$.

2.1. The single layer equation

Standard practice for electrostatic problems is to represent $U(z)$ as a continuous function which is sum of a driving term and a single layer potential [12]

$$U(z) = \Re\left\{\bar{e}z\right\} + \frac{1}{2\pi}\int_\Gamma \rho(\tau)\log|\tau - z|\,\mathrm{d}|\tau|\,, \quad z \in D\,. \tag{7}$$

Here the bar symbol denotes complex conjugation and $\rho(z)$ is an unknown real valued layer density which can be solved from the integral equation

$$\rho(z) + \frac{\lambda(z)}{\pi}\int_\Gamma \rho(\tau)\Im\left\{\frac{n_z\bar{n}_\tau\,\mathrm{d}\tau}{\tau - z}\right\} = 2\lambda(z)\Re\left\{\bar{e}n_z\right\}\,, \quad z \in \Gamma_0\,. \tag{8}$$

This equation is derived by enforcing continuity of normal current across Γ.

Once (8) is solved, the effective conductivity can be computed from

$$\sigma_{\rm eff} = \int_{\Gamma_0}\frac{c(z)}{a(z)}\rho(z)\Re\left\{\bar{e}l_0(z)\right\}\,\mathrm{d}|z|\,. \tag{9}$$

This formula is obtained by rewriting (1) using Green's first identity and it can also be written in a more roundabout way to avoid division with $a(z)$.

2.2. An alternative equation

The single layer potential equation (8) is not the only possibility for the checkerboard problem. An alternative integral equation can be derived by applying Green's third identity to $U(z) - \Re\{\bar{e}z\}$, which is a periodic function. In terms of the transformed potential

$$U^*(z) = U(z)a(z) + \sigma_-(z)\Re\left\{\bar{e}l(z)\right\}\,, \tag{10}$$

this equation assumes a particularly simple form

$$U^*(z) - \frac{\lambda(z)}{\pi}\int_\Gamma U^*(\tau)\Im\left\{\frac{\mathrm{d}\tau}{\tau - z}\right\} = 2\frac{c(z)}{b(z)}\Re\left\{\bar{e}l_0(z)\right\}\,, \quad z \in \Gamma_0\,. \tag{11}$$

The effective conductivity can be computed from

$$\sigma_{\text{eff}} = \int_{\Gamma_0} U^*(z)\Im\left\{\bar{e}\,\mathrm{d}z\right\}\,. \tag{12}$$

This formula is obtained by rewriting (1) using Gauss' theorem.

2.3. The asymptotic behavior of $\rho(z)$ and $U^*(z)$

The behavior of the layer densities $\rho(z)$ of (8) and U^* of (11) close to a checkerboard quadruple-junction depends on the conductivities of the four squares that meet. For some combinations strong singularities can develop.

The worst case is when poorly and well conducting squares meet diagonally like in an two-component ordered checkerboard, see top left image of Fig. 1. Let the poor conductivity be σ_1 and the good conductivity σ_2. Then one can show, with separation of variables, that the density $\rho(z)$ diverges and asymptotically behaves as $s^{\nu-1}$, where s is the distance to the vertex and $0 < \nu \leq 1$ is the smallest positive solution to

$$\frac{\sigma_2}{\sigma_1}\sin^2(\nu\pi/4) = \cos^2(\nu\pi/4)\,. \tag{13}$$

The leading behavior of the density $U^*(z)$ can be described by a constant term plus a term proportional to s^ν.

Note that for large ratios σ_2/σ_1, the strength of the singularity in $\rho(z)$ approaches s^{-1}. For comparison, in a two-wedge corner the worst singularity that can occur is $s^{-0.5}$.

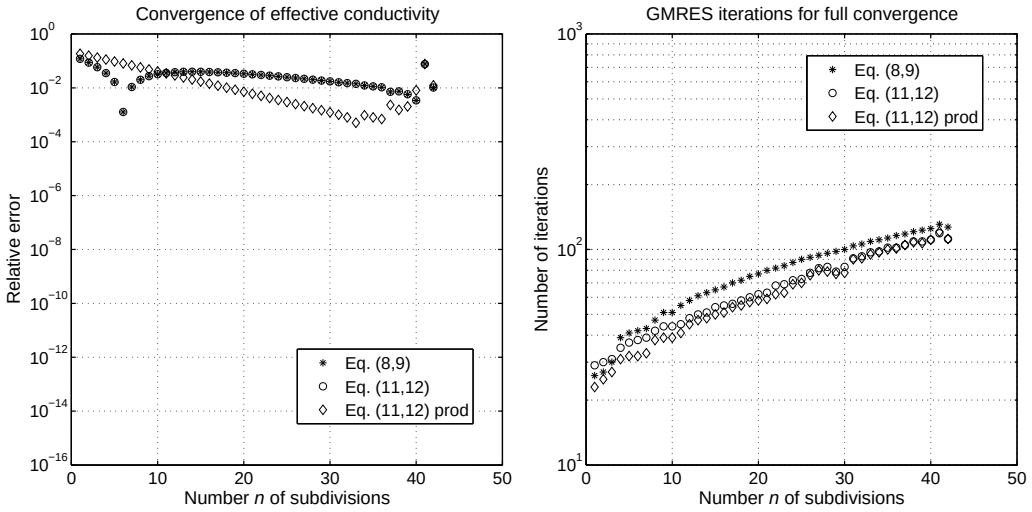

Figure 2: Convergence of the effective conductivity and of the GMRES iterative solver for a two-component ordered checkerboard with $\sigma_2/\sigma_1 = 100$. The diamond symbols indicate that product integration [14] is used for interaction between panels meeting at corner vertices.

2.4. A simple numerical example

We illustrate the properties of (8) and (11) in an example for a two-component ordered checkerboard with $\sigma_2/\sigma_1 = 100$, see top left image of Fig. 1. The unit cell has $N_{\rm sq} = 4$. The exponent of (13) is $\nu \approx 0.127$. An initial mesh with four quadrature panels per square side is deemed sufficient for resolution away from the vertices. The mesh is refined via binary subdivision of panels neighboring vertices as to create a simply graded mesh in the sense of Section 5 of [15].

The convergence of $\sigma_{\rm eff}$ with mesh refinement is illustrated in Fig. 2. The exact result $\sigma_{\rm eff} = \sqrt{\sigma_1\sigma_2}$ [7] is used as reference value. The stars and the circles show that the performance of (8) and (11) are almost identical. The situation is indeed problematic. At 40 subdivisions the shortest panels have lengths of $O(10^{-13})$ and instabilities develop due to the limitations of finite precision arithmetic. By then, we only have achieved convergence to two digits. This is marginally better than the finite element method results of Table 3.1 in Ref. [1].

Fig. 2 also shows that product integration on panels meeting at corner vertices, rather than Gaussian quadrature, can improve the convergence of (11) somewhat. Still, the need for radically better solution methods is obvious.

3. Recursive compressed inverse preconditioning

Recursive compressed inverse preconditioning is a novel and rather general method to deal with the type of problems just encountered (there are other recently developed powerful techniques as well [2]). The idea is to discretize the integral equation on a coarse mesh, further resolve the integral operator locally on a hierarchy of meshes that are refined close to boundary points where singularities occur, invert the operator, and simultaneously compress it onto the coarse grid without the loss of precision using information about the regularity of the right hand side. In this section we give a brief review of how the method works with focus on issues important to its implementation. The machinery for four-wedge corners is very similar to the one developed for three-wedge corners in [15], but we shall use the simplified notation introduced in [16]. See both references for derivations and full definitions.

3.1. Compressed equations

Consider a Fredholm second kind integral equation such as (8) or (11) on the general form

$$(I + K)\,\mu(z) = g(z)\,, \tag{14}$$

where I is the identity, K is an operator which is compact away from corner vertices, $\mu(z)$ is an unknown layer density, and $g(z)$ is a piecewise smooth right hand side.

Let $K(\tau, z)$ denote the kernel of K. Split $K(\tau, z)$ into two functions

$$K(\tau, z) = K^\star(\tau, z) + K^\circ(\tau, z)\,, \tag{15}$$

where $K^\star(\tau, z)$ is zero except for when τ and z simultaneously lie close to the same corner vertex. Then $K^\circ(\tau, z)$ is zero. The kernel split (15) corresponds to an operator split $K = K^\star + K^\circ$ where K° is a compact operator. After discretization, based on a parameterization $z(t)$ and quadrature weights associated with N_p discrete values of the parameter t, (14) assumes the form

$$(\mathbf{I} + \mathbf{K}^\star + \mathbf{K}^\circ)\,\boldsymbol{\mu} = \mathbf{g}\,, \tag{16}$$

where $\mathbf{I}$, $\mathbf{K}^\star$, and $\mathbf{K}^\circ$ are $N_\mathrm{p} \times N_\mathrm{p}$ matrices and $\boldsymbol{\mu}$ and $\mathbf{g}$ are columns vectors with N_p entries. The change of variables

$$\mu(z) = (I + K^\star)^{-1}\,\tilde{\mu}(z) \tag{17}$$

makes (16) read

$$\left(\mathbf{I} + \mathbf{K}^{\circ}\left(\mathbf{I} + \mathbf{K}^{\star}\right)^{-1}\right)\tilde{\boldsymbol{\mu}} = \mathbf{g}\,. \tag{18}$$

This equation corresponds to the discretization of a Fredholm second kind equation with compact operators and the solution $\tilde{\boldsymbol{\mu}}$ is the discretization of a piecewise smooth function.

Now, in (18), $\mathbf{K}^{\circ}$ and $\mathbf{g}$ can be evaluated on a grid on a coarse mesh. Only $(\mathbf{I} + \mathbf{K}^{\star})^{-1}$ needs a grid on a refined mesh for its evaluation. We introduce the compressed weighted inverse

$$\mathbf{R} = \mathbf{P}_W^T\left(\mathbf{I}_{\text{fin}} + \mathbf{K}^{\star}_{\text{fin}}\right)^{-1}\mathbf{P}\,. \tag{19}$$

Here subscript 'fin' indicates the fine grid, $\mathbf{P}$ is a prolongation operator from the coarse grid to the fine grid, $\mathbf{P}_W = \mathbf{W}_{\text{fin}}\mathbf{P}\mathbf{W}_{\text{coa}}^{-1}$ is a weighted prolongation operator, $\mathbf{W}$ is a matrix containing the quadrature weights on the diagonal, and subscript 'coa' indicates the coarse grid, see Section 5 of [16]. Eq. (18) assumes the form

$$\left(\mathbf{I}_{\text{coa}} + \mathbf{K}^{\circ}_{\text{coa}}\mathbf{R}\right)\tilde{\boldsymbol{\mu}}_{\text{coa}} = \mathbf{g}_{\text{coa}}\,, \tag{20}$$

which in terms of the new discrete density $\hat{\boldsymbol{\mu}}_{\text{coa}} = \mathbf{R}\tilde{\boldsymbol{\mu}}_{\text{coa}}$ also can be written

$$\left(\mathbf{I}_{\text{coa}} + \mathbf{R}\mathbf{K}^{\circ}_{\text{coa}}\right)\hat{\boldsymbol{\mu}}_{\text{coa}} = \mathbf{R}\mathbf{g}_{\text{coa}}\,. \tag{21}$$

Functionals on $\mu(z)$ of the type

$$\int f(z)\mu(z)\,\mathrm{d}z = \int f(z(t))\mu(z(t))\,z'(t)\,\mathrm{d}t\,, \tag{22}$$

where $f(z)$ is a piecewise smooth function, assume the discretized form

$$\mathbf{f}_{\text{coa}}^T\mathbf{Z}'_{\text{coa}}\mathbf{W}_{\text{coa}}\mathbf{R}\tilde{\boldsymbol{\mu}}_{\text{coa}}\,, \tag{23}$$

where $\mathbf{f}$ is a column vector and $\mathbf{Z}'$ is a matrix containing discrete values of $z'(t)$ on the diagonal.

3.2. Recursive construction of $\mathbf{R}$

There are N_{sq} four-wedge corner vertices γ_k in D_0. Let $\Gamma_k^{\star}$ be the part of Γ_0 which covers the eight quadrature panels on the coarse mesh that lie closest to γ_k, see Fig. 3. The coarse grid will have 128 discretization points on $\Gamma_k^{\star}$ when 16-point composite quadrature is used. The compressed weighted

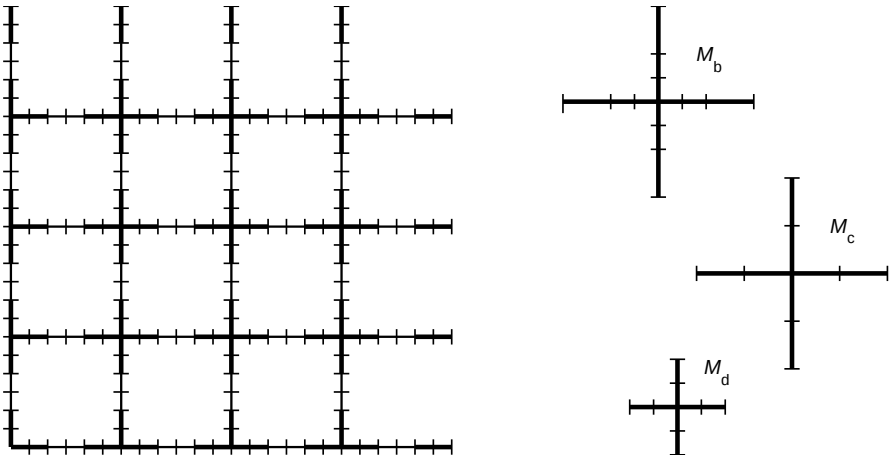

Figure 3: Left: a coarse mesh on Γ_0 for a unit cell with $N_{\rm sq} = 16$. For illustrative purposes there are six quadrature panels on a square side (four are enough in practice). The eight panels forming each $\Gamma_k^\star$ are drawn extra thick. Right: local meshes $\mathcal{M}_{\rm b}$, $\mathcal{M}_{\rm c}$, and $\mathcal{M}_{\rm d}$ are drawn in correct scale relative to each other but magnified compared to the coarse mesh to the left. The $\mathcal{M}_{\rm c}$ mesh coincides with the coarse mesh on $\Gamma_k^\star$. The $\mathcal{M}_{\rm d}$ mesh is a subset of $\mathcal{M}_{\rm b}$. There are 192 discretization points on $\mathcal{M}_{\rm b}$ and 128 points on $\mathcal{M}_c$ and on $\mathcal{M}_d$.

inverse $\mathbf{R}$ corresponds to a block diagonal matrix with $N_{\rm sq}$ blocks $\mathbf{R}_k$ of size 128×128. The remainder of $\mathbf{R}$ is the identity matrix.

The construction of $\mathbf{R}$ from its definition (19) is costly when the refined mesh has many panels on $\Gamma_k^\star$. It may also be unstable. Fortunately, the construction can be greatly sped up and also stabilized via a recursion for each block $\mathbf{R}_k$. This recursion uses grids on local meshes, see Fig. 3, and becomes particularly simple for wedge-like corners thanks to scale invariance of the Cauchy-type integrals in (8) and (11). It assumes the form of a fixed-point iteration where $\mathbf{R}_{nk} \to \mathbf{R}_k$ as $n \to \infty$

$$\mathbf{R}_{ik} = \mathbf{P}_{W\rm bc}^T \left(\mathbb{F}\{\mathbf{R}_{(i-1)k}^{-1}\} + \mathbf{I}_{\rm b}^\circ + \mathbf{K}_{{\rm b}k}^\circ \right)^{-1} \mathbf{P}_{\rm bc}\,, \quad i = 1, \ldots, n\,, \tag{24}$$

initialized with

$$\mathbb{F}\{\mathbf{R}_{0k}^{-1}\} = \mathbf{I}_{\rm b}^\star + \mathbf{K}_{{\rm b}k}^\star\,. \tag{25}$$

Here $\mathbf{K}$ is still the discretization of K and $\mathbf{I}$ is the identity matrix. Subscript k refers to the kth block. The stars and the circles have a meaning which can be explained by considering the discretization of K on a 192-point grid $\mathcal{G}_{\rm b}$ on the mesh $\mathcal{M}_{\rm b}$ and on a 128-point grid $\mathcal{G}_{\rm d}$ which is the subset of $\mathcal{G}_{\rm b}$ on the

mesh $\mathcal{M}_\mathrm{d}$, see Fig. 3. Let the resulting matrices be denoted $\mathbf{K}_\mathrm{b}$ and $\mathbf{K}_\mathrm{d}$. Now $\mathbf{K}_\mathrm{b}^\circ$ is the 192×192 matrix $\mathbf{K}_\mathrm{b}$ with the entries that also are contained in the 128×128 matrix $\mathbf{K}_\mathrm{d}$ set to zero. The matrix $\mathbf{K}_\mathrm{b}^\star$ is defined as $\mathbf{K}_\mathrm{b}^\star = \mathbf{K}_\mathrm{b} - \mathbf{K}_\mathrm{b}^\circ$, that is, $\mathbf{K}_\mathrm{b}^\star$ has the same non-zero entries as $\mathbf{K}_\mathrm{d}$ but is larger. Finally, the operator $\mathbb{F}\{\cdot\}$ expands an 128×128 matrix into an 192×192 matrix by adding zero entries in such a way that $\mathbb{F}\{\mathbf{K}_\mathrm{d}\} = \mathbf{K}_\mathrm{b}^\star$. The 192×128 matrices $\mathbf{P}_\mathrm{bc}$ and $\mathbf{P}_{W\mathrm{bc}}$ are un-weighted and weighted prolongation operators from a grid $\mathcal{G}_\mathrm{c}$ on the mesh $\mathcal{M}_\mathrm{c}$ to $\mathcal{G}_\mathrm{b}$.

3.3. Speedup of the recursion for $\mathbf{R}$

Assume that $\sigma(z)$ is such that ν of Section 2.3 for a vertex γ_k is close to zero. Then the number n of steps needed for convergence in the recursion (24) for the matrix block $\mathbf{R}_k$ may be large. Actually, it grows without bounds as $\nu \to 0$. It could pay off to use a variant of Newton's method.

The recursion (24) can be recast as a non-linear matrix equation

$$F(\mathbf{A}) \equiv \mathbf{A} - \mathbf{P}_{W\mathrm{bc}}^T \left(\mathbb{F}\{\mathbf{A}^{-1}\} + \mathbf{I}_\mathrm{b}^\circ + \mathbf{K}_{\mathrm{b}k}^\circ \right)^{-1} \mathbf{P}_\mathrm{bc} = 0 \,, \tag{26}$$

where $\mathbf{A} = \mathbf{R}_k$. Let $\mathbf{X}$ be a matrix-valued perturbation of $\mathbf{A}$ and expand $F(\mathbf{A} + \mathbf{X}) = 0$ to first order in $\mathbf{X}$. This gives a Sylvester-type matrix equation for $\mathbf{X}$ which can be solved by GMRES or by a variant of the method in [10] (with Schur factorization) and used as a Newton update for $\mathbf{A}$. As initial guess one can take $\mathbf{A} = \mathbf{R}_{0k}$ from (25). For improved speed and precision we use the Schur–Banachiewicz inverse formula for a partitioned matrix [17] when evaluating the inverses in (24) and (26).

One Newton step with GMRES costs about as much as 50 fixed-point iteration steps, but the convergence seems quadratic. As an example we compute $\mathbf{R}_k$ for a $\Gamma_k^\star$ in the two-component ordered checkerboard of Section 2.4 within the single layer formulation (8). With a stopping criterion threshold of $10\epsilon_\mathrm{mach}$ in the relative error $||F(\mathbf{A})||/||\mathbf{A}||$, measured in Frobenius norm, we reach convergence in five Newton steps. This takes 0.34 seconds. Convergence to the same precision with (24) requires 352 fixed-point iteration steps and takes 0.44 seconds.

3.4. Numerical examples with $\mathbf{R}$

We return to the two-component ordered checkerboard of Section 2.4 and see how much improvement recursive compressed inverse preconditioning (20) with (24) gives.

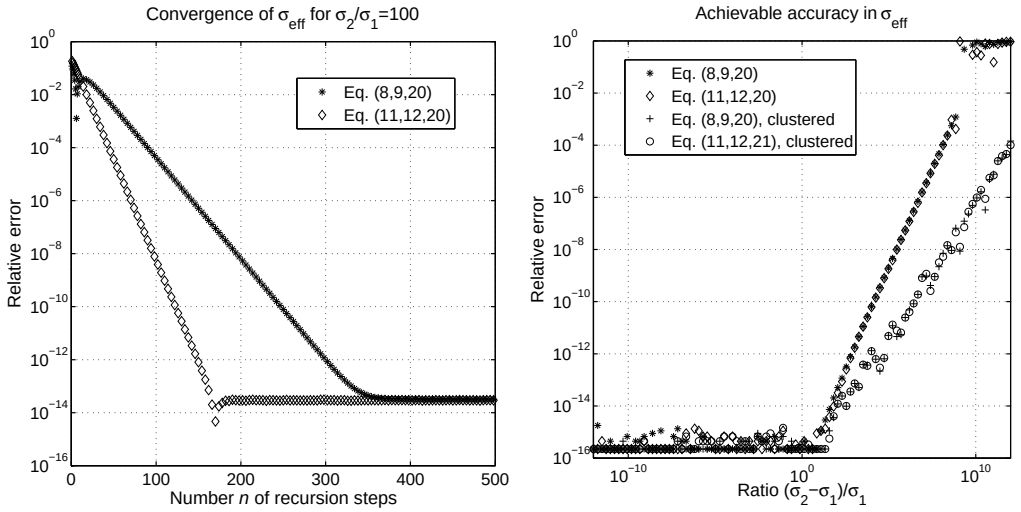

Figure 4: Left: Same as left image of Fig. 2, but recursive compressed inverse preconditioning is used. Right: investigation of achievable accuracy for different conductivity ratios σ_2/σ_1.

The left image of Fig. 4 shows the performance of (8) and (11). Product integration is used in (25) for (11). A comparison with the left image of Fig. 2 shows a dramatic improvement. The recursive compression completely eliminates the instabilities and we can use as many recursion steps (corresponding to subdivisions) as we like. The relative accuracy obtained in σ_{eff} eventually saturates at about 10^{-14}.

As for the preconditioning aspect of recursive compressed inverse preconditioning, the number of GMRES iterations needed for full convergence drops dramatically as well. The alternative equation (11) needs eleven iterations and the single layer equation (8) needs seven iterations, irrespective of the number of recursion steps in (24).

The right image of Fig. 4 illustrates the achievable accuracy in σ_{eff} for various ratios σ_2/σ_1, with $\sigma_2 > \sigma_1$. In these experiments we have limited the number of recursion steps in (24). If convergence, in Frobenius norm and with a stopping criterion threshold of $10\epsilon_{\text{mach}}$, has not occurred in 1000 recursion steps we resort to the Newton iterations of Section 3.3 with a maximum number of 15 iterations and $\mathbf{R}_{1000k}$ as initial guess. This transition occurs at $\sigma_2/\sigma_1 \approx 750$ for (8) and at $\sigma_2/\sigma_1 \approx 3200$ for (11). Fig. 4 shows that there are no cancellation effects as $\sigma_2/\sigma_1 \to 1$, but precision is lost at a rate of about

$(\sigma_2/\sigma_1)^{1.5}$ as $\sigma_2/\sigma_1 \to \infty$. Fig. 4 also shows that extra clustering of some quadrature points on panels that lie closest to the γ_k, in a direction towards γ_k, and replacing (20) with (21) for (11) greatly increases the achievable accuracy for very high ratios σ_2/σ_1.

We end this section with an example for the multi-component random checkerboard with $N_{\text{sq}} = 16$ shown in the bottom left image of Fig. 1. The conductivities are $\sigma_1 = 0.002$, $\sigma_2 = 3$, $\sigma_3 = 30$, $\sigma_4 = 300$, $\sigma_5 = 700$, $\sigma_6 = 0.004$, $\sigma_7 = 400$, $\sigma_8 = 3$, $\sigma_9 = 0.5$, $\sigma_{10} = 0.4$, $\sigma_{11} = 900$, $\sigma_{12} = 0.2$, $\sigma_{13} = 0.003$, $\sigma_{14} = 0.2$, $\sigma_{15} = 10$, and $\sigma_{16} = 200$. Here we have no exact reference value for σ_{eff} in the y-direction, but the results for produced by (8) with (9) and by (11) with (12) agree to thirteen digits ($\sigma_{\text{eff}} = 26.93379911313$) thereby illustrating the consistency of the two formulations in a more ambitious setting. Both formulations need 25 GMRES iterations for convergence.

4. Long-range preconditioning

As the number of squares in the unit cell of a random checkerboard grows, the problem of computing its effective conductivity gets harder. For one thing, the number of iterations needed to solve the discretized equations to a given accuracy grows. This phenomenon, due to long-range interaction, is well-known [8] and is illustrated in Fig. 16 of [15] for an aggregate of grains with conductivity ratios up to 10^6. The largest geometry that could be treated there, due to memory constraints, has 900 grains in the unit cell. Around 700 GMRES iterations are needed for convergence. This is bad. Not only does it take time and requires a lot of memory. The achievable accuracy also suffers. This section describes a preconditioner which, roughly speaking, will increase the overall efficiency of such computations with a factor of at least ten. We concentrate on equation (11) with (20), which has shown the best performance so far for low and medium high ratios σ_2/σ_1.

The idea behind our preconditioner is to split the unknown $U^*(z)$ of (11) into two parts. One part will mimic the average local behavior of $U^*(z)$ with few degrees of freedom. The other part will mimic the rapidly varying behavior of $U^*(z)$ with many degrees of freedom. We seek to expand the integral equation as to decouple the two parts of $U^*(z)$ as much as possible, hoping that the ill-conditioning due to long-range interaction will be captured by equations for the average local behavior. Then we use systems of such equations as a preconditioner for the original equation.

4.1. An expanded equation

Each square in D_0 has a boundary consisting of four straight segments, two of which have positive orientation relative to the square, and two of which have negative orientation relative to the square, see Fig. 1. Introduce piecewise constant local basis functions $s_k(z)$, $k = 1, \ldots, N_{\rm sq}$, on $\Gamma_0 \cup \Gamma_2$ such that $s_k(z) = 1$ when z lies on a boundary part of square k with positive orientation, $s_k(z) = -1$ when z lies on a boundary part of square k with negative orientation, and $s_k(z) = 0$ otherwise.

Let us take (11) on the general form (14), where $\mu(z)$ corresponds to $U^*(z)$, and make the split

$$\mu(z) = \mu_0(z) + \sum_{k=1}^{N_{\rm sq}-1} a_k s_k(z)\,. \tag{27}$$

Here a_k are coefficients and

$$\int s_k(z)\mu_0(z)\,\mathrm{d}|z| = 0\,, \quad k = 1, \ldots, N_{\rm sq} - 1\,. \tag{28}$$

The last square in the unit cell is excluded from the sum in (27) in order to break symmetry and to make the a_k unique.

The particular choice of local basis functions $s_k(z)$ is motivated, in part, by that the action of K in (11) on $s_k(z)$ can be evaluated analytically and that the result is a chiefly local function

$$Ks_k(z) = -\lambda(z)|s_k(z)| + \frac{2\lambda(z)}{N_{\rm sq}}\,. \tag{29}$$

Using (27) and (29) we rewrite (14) as

$$(I + K)\,\mu_0(z) + \sum_{k=1}^{N_{\rm sq}-1} a_k \left(s_k(z) - \lambda(z)|s_k(z)| + \frac{2\lambda(z)}{N_{\rm sq}} \right) = g(z)\,. \tag{30}$$

Discretization of (30) and (28) together with recursive compressed inverse preconditioning applied to $\mu_0(z)$ results in the linear system

$$(\mathbf{I}_{\rm coa} + \mathbf{K}^{\circ}_{\rm coa}\mathbf{R})\,\tilde{\boldsymbol{\mu}}_{0\rm coa} + \left(\mathbf{B}_1 - \boldsymbol{\Lambda}_{\rm coa}|\mathbf{B}_1| + \boldsymbol{\lambda}_{\rm coa}\mathbf{u}^T\right)\mathbf{a} = \mathbf{g}_{\rm coa}\,, \tag{31}$$

$$\mathbf{B}_1^T\mathbf{W}_{\rm coa}|\mathbf{Z}'_{\rm coa}|\mathbf{R}\tilde{\boldsymbol{\mu}}_{0\rm coa} = \mathbf{0}\,. \tag{32}$$

Here $\mathbf{B}_1$ is a $N_\mathrm{p} \times (N_\mathrm{sq}-1)$ matrix whose kth column is the discretization of $s_k(z)$, $\boldsymbol{\lambda}$ is a column vector whose N_p entries is the discretization of $\lambda(z)$, $\boldsymbol{\Lambda}$ is matrix containing $\boldsymbol{\lambda}$ on the diagonal, $\mathbf{u}$ is a column vector with $N_\mathrm{sq}-1$ entries all equal to $2/N_\mathrm{sq}$, $\mathbf{a}$ is a column vector containing the $N_\mathrm{sq}-1$ coefficients a_k, and vertical bars denote entrywise absolute value.

The effective conductivity (12) can be computed from

$$\sigma_\mathrm{eff} = \Im\left\{\bar{\mathbf{e}}_\mathrm{coa}^T \mathbf{Z}'_\mathrm{coa} \mathbf{W}_\mathrm{coa} \left(\mathbf{R}\tilde{\boldsymbol{\mu}}_{0\mathrm{coa}} + \mathbf{B}_1\mathbf{a}\right)\right\}, \tag{33}$$

once (31) and (32) is solved. Compare (23).

4.2. A Schur complement style preconditioner

The system (31) and (32) can be written in partitioned form

$$\begin{bmatrix} \mathbf{I}+\mathbf{K}^\circ\mathbf{R} & \mathbf{B} \\ \mathbf{C} & \mathbf{0} \end{bmatrix} \begin{bmatrix} \tilde{\boldsymbol{\mu}}_0 \\ \mathbf{a} \end{bmatrix} = \begin{bmatrix} \mathbf{g} \\ 0 \end{bmatrix}, \tag{34}$$

where subscripts 'coa' are omitted and

$$\mathbf{B} = \mathbf{B}_1 - \boldsymbol{\Lambda}_\mathrm{coa}|\mathbf{B}_1| + \boldsymbol{\lambda}_\mathrm{coa}\mathbf{u}^T, \tag{35}$$

$$\mathbf{C} = \mathbf{B}_1^T \mathbf{W}_\mathrm{coa}|\mathbf{Z}'_\mathrm{coa}|\mathbf{R}. \tag{36}$$

The change of variables

$$\begin{bmatrix} \tilde{\boldsymbol{\mu}}_0 \\ \mathbf{a} \end{bmatrix} = \begin{bmatrix} \mathbf{I} & \mathbf{B} \\ \mathbf{C} & \mathbf{0} \end{bmatrix}^{-1} \begin{bmatrix} \boldsymbol{\omega}_1 \\ \boldsymbol{\omega}_2 \end{bmatrix} = \begin{bmatrix} \mathbf{I}-\mathbf{B}\mathbf{S}^{-1}\mathbf{C} & \mathbf{B}\mathbf{S}^{-1} \\ \mathbf{S}^{-1}\mathbf{C} & -\mathbf{S}^{-1} \end{bmatrix} \begin{bmatrix} \boldsymbol{\omega}_1 \\ \boldsymbol{\omega}_2 \end{bmatrix}, \tag{37}$$

where the $(N_\mathrm{sq}-1)\times(N_\mathrm{sq}-1)$ matrix block $\mathbf{S}$ is given by

$$\mathbf{S} = \mathbf{C}\mathbf{B}, \tag{38}$$

transforms (34) into

$$\begin{bmatrix} \mathbf{I}+\mathbf{K}^\circ\mathbf{R}(\mathbf{I}-\mathbf{B}\mathbf{S}^{-1}\mathbf{C}) & \mathbf{K}^\circ\mathbf{R}\mathbf{B}\mathbf{S}^{-1} \\ \mathbf{0} & \mathbf{I} \end{bmatrix} \begin{bmatrix} \boldsymbol{\omega}_1 \\ \boldsymbol{\omega}_2 \end{bmatrix} = \begin{bmatrix} \mathbf{g} \\ 0 \end{bmatrix}. \tag{39}$$

Obviously, $\boldsymbol{\omega}_2 = \mathbf{0}$ and we can write (39) as a single equation for $\boldsymbol{\omega}_1$:

$$\left(\mathbf{I}+\mathbf{K}^\circ\mathbf{R}(\mathbf{I}-\mathbf{B}\mathbf{S}^{-1}\mathbf{C})\right)\boldsymbol{\omega}_1 = \mathbf{g}. \tag{40}$$

4.3. The inverse of $\mathbf{S}$

Note that $\mathbf{C}$ of (36) is a sparse $(N_{\rm sq}-1)\times N_{\rm p}$ matrix and that $\mathbf{B}$ of (35) is a sum of three matrices, two of which have the same sparsity pattern and the third is rank one. This makes $\mathbf{S}$ of (38) a sum of a sparse matrix (a *lattice operator*) and a rank one matrix. In the limit $\lambda(z)\to 0$, the matrix $\mathbf{S}$ approaches a standard five-point stencil for the discrete Laplace operator. Most rows and columns of the lattice operator, for general $\lambda(z)$, have nine non-zero entries. The columns, then, sum up to zero. The rows and columns corresponding to squares (or periodic images of squares) that neighbor the $N_{\rm sq}$th square have eight non-zero entries. In the right image of Fig. 1 such squares have numbers 1, 3, 4, 9, 11, 12, 13, and 15. The entries of the lattice operator can be computed in $O(N_{\rm sq})$ time.

Solving linear systems with $\mathbf{S}$ as system matrix using LU-factorization is no problem on a modern workstation for $N_{\rm sq}$ up to about 10^4 and we shall use this method here. The time it takes is small compared to the time other computational tasks take in our algorithm. The storage required for the factorization is, at $N_{\rm sq}=10^4$, comparable to the storage required for quantities such as the matrix blocks $\mathbf{R}_k$. Besides, the LU-factorization only has to be carried out once. Still, should one wish to study much larger checkerboards, LU-factorization is no longer an option. We speculate that some kind of hierarchical iterative solver for $\mathbf{S}$-systems, perhaps multigrid, could be one way to go. The fast direct nested dissection scheme of Martinsson [19] is surely also an interesting option.

4.4. Numerical examples with long-range preconditioning

This section tests the combination of recursive compressed inverse preconditioning and long-range preconditioning, that is (40) with (37) and (33). We begin with the the multi-component random checkerboard shown in the bottom left image of Fig. 1 and already solved in Section 3.4. Again we get $\sigma_{\rm eff}=26.93379911313$, which illustrates the consistency of the new formulation with the previous ones. The number of iterations needed for convergence in GMRES, however, drops from 25 in Section 3.4 to 16.

As a main test we construct a series of progressively larger setups, $4\le N_{\rm sq}\le 10,609$, where the conductivities are given by $\sigma_k=10^{c_k}$, with c_k being a random variable uniformly distributed in $[-3,3]$. A checkerboard with $N_{\rm sq}=10^4$ such squares in the unit cell is depicted in Fig.5.

The difference between using the recursive compressed inverse preconditioning of Section 3 only, and recursive compressed inverse preconditioning

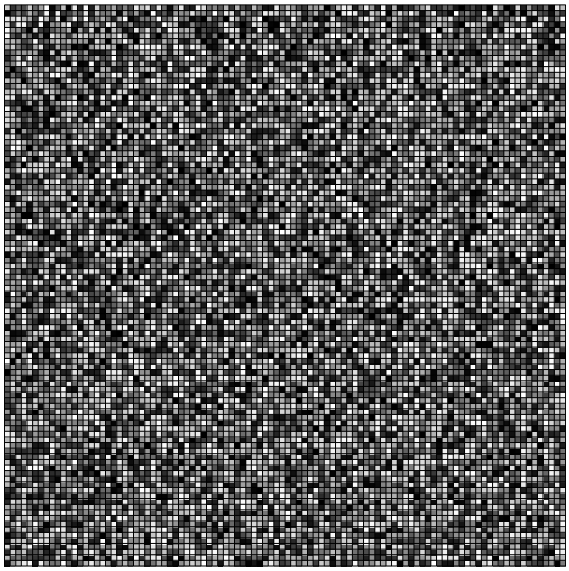

Figure 5: A unit cell with 10,000 squares of a multi-component random checkerboard. The conductivity varies between $\sigma = 0.001$ (darkest) and $\sigma = 1000$ (lightest).

together with long-range preconditioning is remarkable. Especially so for unit cells with a large number of squares. Fig. 6 shows that without long-range preconditioning the number of GMRES iterations needed for convergence grows at an alarming rate, compare Fig. 16 of Ref. [15], making computations for $N_{\rm sq} > 10^3$ exceedingly slow and unreliable, if not impossible. With long-range preconditioning the number of GMRES iterations seems bounded by 21. It appears as if our preconditioner has captured the long-range interaction completely.

Fig. 6 also shows an attempt at error estimation. Lacking exact results for $\sigma_{\rm eff}$, we construct reference solutions by doubling the number of panels on each square side on the coarse mesh from four to eight. The estimated relative error presented in Fig. 6 is the relative difference between the results produced with the two meshes. The growth of the relative error with $N_{\rm sq}$ is moderate and we conclude that accurate solutions of large multi-component random checkerboards at high conductivity ratios indeed can be produced.

As for timings, we quote the following for $N_{\rm sq} = 10^4$ squares and $N_{\rm p} = 1.28 \cdot 10^6$ discretization points in the unit cell D_0: Construction of $\mathbf{R}$ takes 20 minutes, construction and LU-factorization of $\mathbf{S}$ takes 3 minutes, iterative

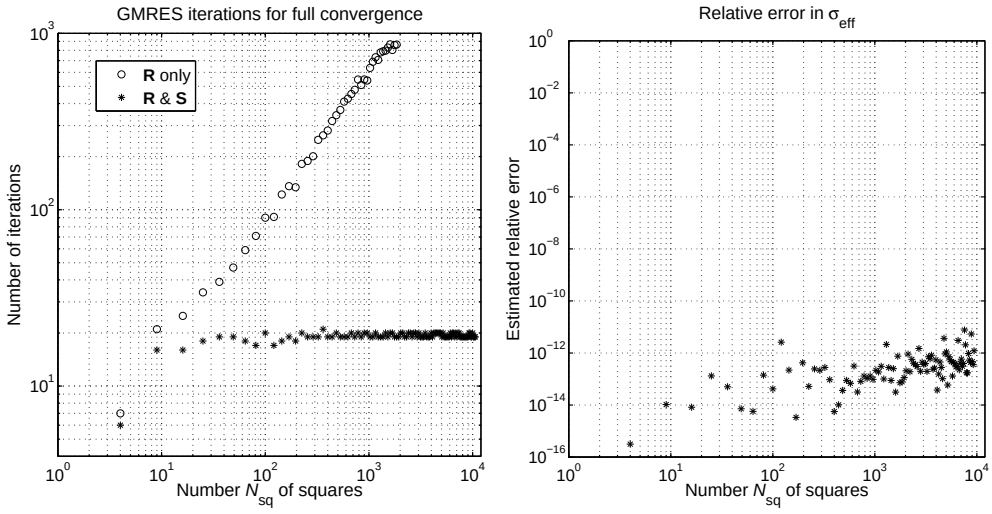

Figure 6: Left: the number of GMRES iterations needed for full convergence in the linear system, resulting from the discretization of (11), as a function of checkerboard size $N_{\rm sq}$. The use of recursive compressed inverse preconditioning only, denoted '$\mathbf{R}$ only', is compared with use of the long-range preconditioning as well, denoted '$\mathbf{R}$ & $\mathbf{S}$'. Right: error estimates for the effective conductivity.

solution of (40) takes 14 minutes.

5. Discussion

The problem of computing the effective conductivity of large random checkerboards at high conductivity ratios is difficult and, seemingly, hopelessly ill-conditioned in various ways. Much recent research has therefore been directed towards finding closed-form solutions for models with a small number of squares or rhombuses in the unit cell. This paper shows that checkerboard problems can be solved efficiently and to high precision using purely numerical techniques, at least, say, for conductivity ratios up to 10^8 and for unit cells with up to 10^4 squares.

Two issues should be addressed if one wishes to push the limits further with respect to achievable accuracy and tractable system size within the framework of the present method. First, a fast solver is needed for linear systems involving the matrix $\mathbf{S}$ of (38). Some ideas on how to proceed were discussed in Section 4.3. The second issue is the rate with which

precision is lost as the conductivity ratio $\sigma_2/\sigma_1 \to \infty$ for an ordered two-component checkerboard. This rate controls the achievable accuracy also for larger random checkerboards. We observed, in Section 3.4, that the rate was $(\sigma_2/\sigma_1)^{1.5}$. This reflects the conditioning of the matrix equation (26) when Legendre nodes are used for discretization and feels rather on the high side considering that the condition number of the $\mathbf{R}$ matrix, where much of the ill-conditioning of the underlying integral equations is contained, appears to grow at a rate of only $(\sigma_2/\sigma_1)^{0.5}$. Other choices of discretization points on panels neighboring corner vertices and replacing (20) with (21) can improve the situation in this respect, as shown in the right image of Fig. 4.

References

[1] S.A. Berggren, D. Lukkassen, A. Meidell, L. Simula, A new method for numerical solution of checkerboard fields, J. Appl. Math., **1**(4), 157–173 (2001).

[2] J. Bremer and V. Rokhlin, Efficient discretization of Laplace boundary integral equations on polygonal domains, J. Comput. Phys., **229**(7), 2507–2525 (2010).

[3] M. Briane and Y. Capdeboscq, Expansion formulae for the homogenized determinant of anisotropic checkerboards, Proc. R. Soc. Lond. A, **462**(2073), 2759–2779, (2006).

[4] Y. Chen and C.A. Schuh, Effective transport properties of random composites: Continuum calculations versus mapping to a network, Phys. Rev. E, **80**(4), 040103 (2009).

[5] R.V. Craster and Y.V. Obnosov, A three-phase tessellation: solution and effective properties, Proc. R. Soc. Lond. A, **460**(2044) 1017–1037 (2004).

[6] R.V. Craster and Y.V. Obnosov, A model four-phase checkerboard structure, Q. Jl. Mech. Appl Math., **59**(1) 1–27 (2006).

[7] A.M. Dykhne, Conductivity of a two-dimensional two-phase system, Sov. Phys. JETP, **32**(1) 63–65 (1971).

[8] R.G. Edwards, J. Goodman, and A.D. Sokal, Multigrid method for the random-resistor problem, Phys. Rev. Lett., **61**(12), 1333–1335 (1988).

[9] L.G. Fel and I.V. Kaganov, Relation between effective conductivity and susceptibility of two-component rhombic checkerboard, J. Phys. A, **36**(19), 5349–5358 (2003).

[10] J.D. Gardiner, A.J. Laub, J.J. Amato, and C.B. Moler, Solution of the Sylvester Matrix equation $AXB^T + CXD^T = E$, ACM Trans. Math. Software, **18**(2), 223–231 (1992).

[11] L. Greengard and M.C. Kropinski, Integral equation methods for Stokes flow in doubly-periodic domains, J. Eng. Math. **48**(2), 157–170 (2004).

[12] L. Greengard and J.-Y. Lee, Electrostatics and heat conduction in high contrast composite materials, J. Comput. Phys., **211**(1), 64–76 (2006).

[13] L. Greengard and V. Rokhlin, A fast algorithm for particle simulations, J. Comput. Phys., **73**(2), 325–348 (1987).

[14] J. Helsing and R. Ojala, On the evaluation of layer potentials close to their sources, J. Comput. Phys., **227**(5), 2899–2921 (2008).

[15] J. Helsing and R. Ojala, Corner singularities for elliptic problems: Integral equations, graded meshes, quadrature, and compressed inverse preconditioning, J. Comput. Phys., **227**(20), 8820–8840 (2008).

[16] J. Helsing, Integral equation methods for elliptic problems with boundary conditions of mixed type, J. Comput. Phys., **228**(23), 8892–8907, (2009).

[17] H.V. Henderson and S.R. Searle, On deriving the inverse of a sum of matrices, SIAM Rev., **23**(1), 53–60 (1981).

[18] J.B. Keller, A theorem on the conductivity of a composite medium, J. Math. Phys., **5**(4), 548–549 (1964).

[19] P.G. Martinsson, A fast direct solver for a class of elliptic partial differential equations, J. Sci. Comput., **38**(3), 316–330, (2009).

[20] K.S. Mendelson, A theorem on the effective conductivity of two-dimensional heterogeneous medium, J. Appl. Phys., **46**(11), 4740–4741 (1975).

[21] G.W. Milton, Proof of a conjecture on the conductivity of checkerboards, J. Math. Phys., **42**(10), 4873–4882 (2001).

[22] Y.N. Ovchinnikov, Conductivity of a periodic two-component system of rhombic type, J. Exp. Theor. Phys., **98**(1) 162–169 (2004).

[23] Y. Saad and M.H. Schultz, GMRES: A generalized minimal residual algorithm for solving nonsymmetric linear systems, SIAM J. Sci. Stat. Comp., **7**(3), 856–869 (1986).

[24] E. Tuncer, Y.V. Serdyuk, and S.M. Gubanski, Dielectric mixtures: Electrical properties and modeling, IEEE Trans. Diel. Electr. Insul., **9**(5), 809–828 (2002).